Single-crystal Magnetic Properties of Lanthanide Complexes. Part VIII.[1] Hexakis(antipyrine)praseodymium(III) Tri-iodide

By **M. Gerloch** * and **D. J. Mackey**, University Chemical Laboratory, Lensfield Road, Cambridge CB2 1EW

The principal and average magnetic moments of hexakis(antipyrine)praseodymium(III) tri-iodide (antipyrine is 2,3-dimethyl-1-phenyl-Δ^3-pyrazolin-5-one), have been measured in the temperature range 300—80 K. The temperature dependence of the anisotropy $\chi_{\parallel} - \chi_{\perp}$ is unusual compared with other lanthanide ions in this series, but is directly reproduced by the same D_{3d} point-charge crystal-field model used previously. Calculations have used a $^3H_4 + {}^3H_5$ free-ion basis corrected for the effects of intermediate coupling. Selected calculations show that inclusion of the complete ^3H and ^3F terms in the basis is unnecessary. Values of ρ_4 and ρ_6, the fourth and sixth-order radial parameter, are estimated both to lie in the range 600 ± 100 cm^{-1}. A value for $A_2\langle r^2\rangle$ related to the second-order term in the potential, is estimated as 290 ± 50 cm^{-1}.

We report here studies of the single-crystal and powder magnetic properties of hexakis(antipyrine)praseodymium(II) tri-iodide, $Pr(antip)_6I_3$ (where antip = antipyrine = 2,3-dimethyl-1-phenyl-Δ^3-pyrazolin-5-one), being the f^2 member of this series of trigonally distorted octahedral[2] lanthanide complexes. Free-ion eigenvalues for the states of praseodymium(III) have been estimated from observed spectra of the chloride, ethyl sulphate, and double nitrate and fitted by a least-squares procedure to an intermediate-coupling model.[3] Table 1 lists eigenvalues and purities of the associated eigenvectors for the lowest two Russell–Saunders terms. The lowest-lying state above these is a $^1G_4$

[1] Part VII, M. Gerloch and D. J. Mackey, *J.C.S. Dalton*, 1972, 42.

[2] R. W. Baker and J. W. Jeffery, *Acta Cryst.*, 1969, A,XIV 16 (*Stony Brook Internat. Union Cryst. Abs.*, 1969); R. W. Baker, personal communication.

[3] W. A. Runciman and B. G. Wybourne, *J. Chem. Phys.*, 1959, **31**, 1149.

state at *ca.* 9500 cm^{-1}. Unlike the thulium(III) analogue,[4] the ordering of states follows a Landé splitting rule and quantitatively the smaller spin–orbit coupling coefficient of praseodymium(III) greatly reduces the effects of

TABLE 1

Lowest eigenvalues and eigenvector purities for f^2

State	$^3H_4$	$^3H_5$	$^3H_6$	$^3F_2$	$^3F_3$	$^3F_4$
Energy	0	2171	4274	4950	6327	6770
% Purity	97	100	99	97	100	75

intermediate coupling. Our calculations of crystal-field splittings in D_{3d} symmetry and of the resultant magnetic moments use the first two states, $^3H_4$ and $^3H_5$, as basis, corrected for intermediate coupling as in the Appendix. Some later checks using the 54 × 54 matrix of the ^3H and ^3F terms complete, show that the restricted basis set is accurate to better than one percent. As usual the point-charge crystal-field model is parameterized by ρ_2, ρ_4, and ρ_6 for second-, fourth-, and sixth-order radial integrals, and θ, the distortion angle subtended by an effective Pr–O bond and the 3-fold molecular axis.

EXPERIMENTAL

Powder susceptibilities and crystal anisotropies of Pr(antip)$_6$I$_3$ were measured in the temperature range 80—300 K by the Gouy and Krishnan ' critical torque ' techniques, respectively. The results, corrected for the diamagnetic properties of the lutetium analogue,[5] are given in Tables 2 and 3. The anisotropy $\chi_{\parallel} - \chi_{\perp}$ appears to have an unusual temperature dependence, for while $\Delta\chi$ values of other members of this series rise steadily with decreasing temperature, $\Delta\chi$ for this praseodymium compound reaches a maximum as shown in Figure 1(*a*). We

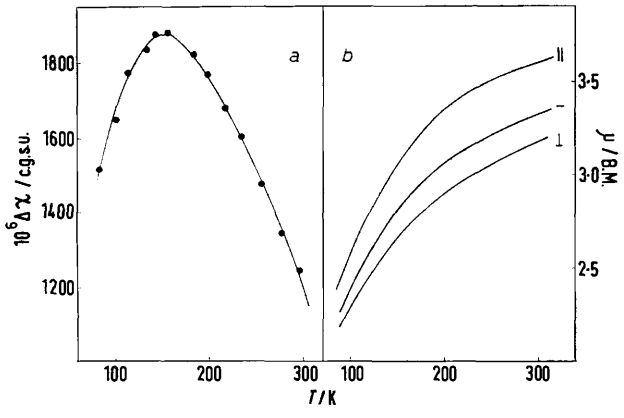

FIGURE 1 (*a*) Experimental anisotropy of Pr(antip)$_6$I$_3$. (*b*) Principal and average moments of Pr(antip)$_6$I$_3$

have checked our results by repetition on a second sample prepared from an alternative source of praseodymium oxide (Pr_6O_{11}) and find the results are reproducible within experimental error. Further, analysis of our sample of Pr(antip)$_6$I$_3$ by Johnson, Matthey and Co. were satisfactory for praseodymium, and concentrations of other rare earths did not exceed 600 p.p.m. The largest impurity was neodymium at 30 p.p.m. and as Nd(antip)$_6$I$_3$ has a moment of *ca.* 3·5 B.M., the results in Table 3 and Figure 1(*a*) appear to be reliable. The maximum in $\Delta\chi$ does not necessarily imply any magnetic exchange effects, of course, as is seen most readily from plots of the principal moments in Figure 1(*b*). It is, nevertheless, important to see if this ' anomalous ' behaviour is reproduced by the same point-change model we have used successfully elsewhere in the series.

Interpolated principal and average moments are given in Table 4.

TABLE 2

Experimental average molecular susceptibilities of Pr(antip)$_6$I$_3$

T/K	$10^6\bar{\chi}'_M$ / c.g.s.u. mol^{-1}	T/K	$10^6\bar{\chi}'_M$ / c.g.s.u. mol^{-1}
303·0	4600	207·0	5780
293·5	4690	192·0	5990
288·5	4720	174·0	6240
281·0	4820	161·0	6490
276·0	4880	144·5	6680
272·5	4910	130·0	6900
255·5	5120	115·0	7010
238·0	5340	101·0	7140
223·5	5530	90·0	7230

TABLE 3

Experimental molecular anisotropies of Pr(antip)$_6$I$_3$

T/K	$10^6(\chi_{\parallel} - \chi_{\perp})$ / c.g.s.u. mol^{-1}	T/K	$10^6(\chi_{\parallel} - \chi_{\perp})$ / c.g.s.u. mol^{-1}
295·5	1245	156·5	1880
276·5	1345	143·0	1875
255·0	1475	133·5	1835
234·5	1605	113·5	1775
217·0	1680	100·5	1650
198·5	1770	83·0	1515
183·5	1825		

TABLE 4

Interpolated magnetic moments of Pr(antip)$_6$I$_3$

T/K	$\bar{\mu}$/B.M.	$\mu_{\parallel}$/B.M.	$\mu_{\perp}$/B.M.
303·0	3·34	3·62	3·20
293·5	3·32	3·60	3·17
288·5	3·30	3·59	3·15
281·0	3·29	3·57	3·13
276·0	3·28	3·57	3·13
272·5	3·27	3·57	3·11
255·5	3·23	3·53	3·07
238·0	3·19	3·49	3·03
223·5	3·15	3·44	2·98
207·0	3·10	3·39	2·94
192·0	3·04	3·32	2·88
174·0	2·98	3·22	2·80
161·0	2·89	3·16	2·75
144·5	2·78	3·03	2·65
130·0	2·68	2·91	2·56
115·0	2·54	2·75	2·43
101·0	2·40	2·58	2·31
90·0	2·28	2·46	2·21

DISCUSSION

Figure 2 shows energies of the crystal-field components of the two lowest states as functions of θ for values of ρ_2, ρ_4, and ρ_6 which are representative of the subsequent fit to magnetic moments. There is usually an A_{1g} non-magnetic ground-state except for highly distorted trigonal elongations. When $\theta < 47°$ for the conditions of Figure 2, or when $\theta < 49°$ for $\rho_4 = 500$, $\rho_6 = 200$ cm^{-1}, say, the ground-state becomes E_g. As seen

[4] M. Gerloch and D. J. Mackey, *J.C.S. Dalton*, 1972, 37.
[5] M. Gerloch and D. J. Mackey, *J. Chem. Soc.* (*A*), 1970, 3040.

later, the magnetic properties vary smoothly through the octahedral angle and, as usual, the sign of magnetic anisotropy is determined by the sign of angular distortion: this is so despite the ' asymmetric ' appearance

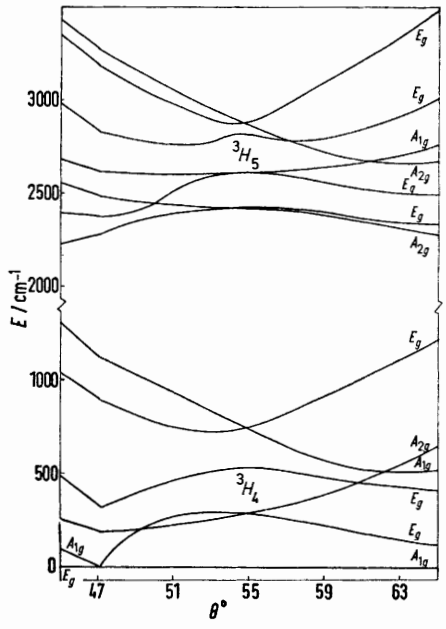

FIGURE 2 Calculated energy levels of lowest two states of the f^2 configuration as functions of θ. $\rho_2 = 1500$, $\rho_4 = 600$, $\rho_6 = 600$ cm^{-1}

of the ground-state cross-over with respect to θ_{oct}. We have noted similar behaviour for the terbium [6] and thulium [4] analogues although in those cases the first excited- and ground-state were very close throughout the angular range. The crossing of the E_g and A_{1g} ground-state around θ *ca.* 49° appears from the

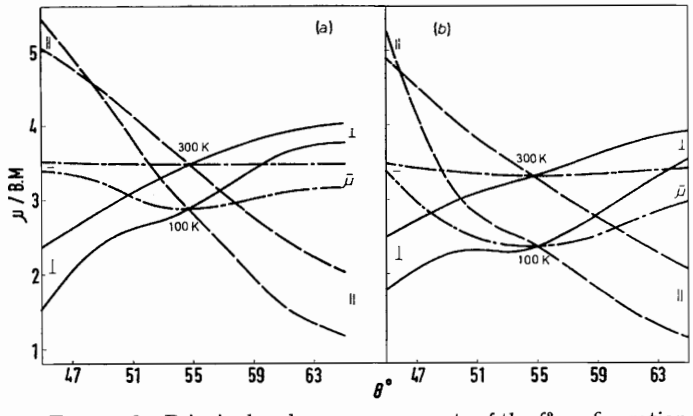

FIGURE 3 Principal and average moments of the f^2 configuration as functions of θ and temperature calculated (*a*) for $\rho_2 = 1500$, $\rho_4 = 500$, $\rho_6 = 200$ cm^{-1} and (*b*) $\rho_2 = 1500$, $\rho_4 = 600$, $\rho_6 = 600$ cm^{-1}. Solid lines $\mu_\perp$, dashed lines $\mu_\parallel$, and dot-dashed lines $\bar{\mu}$

large interactions between the three E_g states of the $^3E_4$ free-ion state.

In Figure 3 we plot principal and average magnetic moments of the f_2 system as functions of θ for two sets of ρ_4 and ρ_6 values. Those in Figure 3(*a*) were chosen on the basis of ' expected ' values for ρ_4 and ρ_6; those in 3(*b*) by final fitting of them to experiment. Considering Figure 3(*a*) first, we note the usual independence of $\bar{\mu}$(300 K) on θ, and also the smooth variations of $\mu_\parallel$ and $\mu_\perp$ at 300 K. The calculations for 100 K, however, are somewhat unusual. Although $\mu_\parallel$(100 K) varies smoothly through the angular range, $\mu_\perp$(100 K) shows a change in curvature for θ values near 51°, presumably associated with the change in ground-state noted above. More important is that $\bar{\mu}$(100) varies much more with θ than in other f^n configurations so far studied in this series. The temperature variation of $\bar{\mu}$ near θ_{oct} is also larger—certainly as a percentage—than for other f^n systems. Many of these points are amplified for the conditions of Figure 3(*b*) where we take $\rho_4 = 600$, $\rho_6 = 600$ cm^{-1}. In particular, the temperature variation of $\bar{\mu}$ near θ_{oct} has approximately doubled with respect to the conditions of Figure 3(*a*).

Our usual procedure for fitting the experimental magnetic moments in this series rests on the independence of the mean moments on θ (near perfect at 300 K and approximate at 100 K), but as these conditions

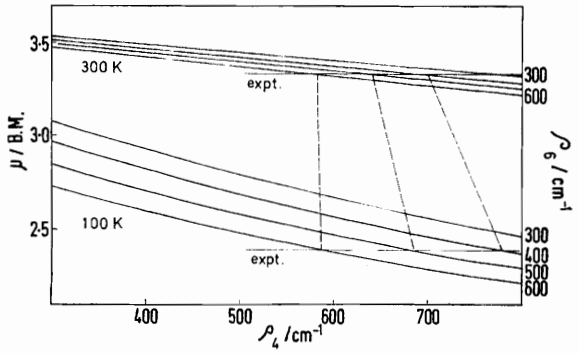

FIGURE 4 Calculated mean moments as functions of ρ_4 and ρ_6. Experimental values for Pr(antip)$_6$I$_3$ are shown at 300 and 100 K. Dotted lines indicate procedure for obtaining simultaneous fits at both temperatures. $\rho_2 = 1500$ cm^{-1}, $\theta = 53°$

are much less apparent in the f^2 system we have adopted an iterative procedure. We begin by assuming a fit for θ *ca.* 53°, in common with other members of the series. At this angle we plot mean moments at 100 and 300 K as functions of ρ_4 for a set of ρ_6 values, as in Figure 4. Average moments are about equally dependent upon changes in ρ_4 and ρ_6 being more sensitive at 100 than 300 K. Experimental values for Pr(antip)$_6$I$_3$ are shown and simultaneous fits for 300 and 100 K are obtained for ρ_4 *ca.* 600 and ρ_6 *ca.* 600 cm^{-1}. The fitting process is shown more clearly by Figure 5(*a*) in which ρ_4 values are plotted against ρ_6 for combinations giving perfect fits to $\bar{\mu}$(300 K) and $\bar{\mu}$(100 K), independently. The curves intersect at $\rho_4 = 560$, $\rho_6 = 620$ cm^{-1} for simultaneous fit at 300 and 100 K. For interest, we include corresponding curves calculated with neglect of intermediate coupling (see Appendix): these curves

[6] M. Gerloch and D. J. Mackey, *J. Chem. Soc.* (*A*), 1971, 2605.

intersect at $\rho_4 = 590$, $\rho_6 = 540$ cm^{-1}. Bearing in mind an experimental error of $\pm 1\%$ in observed $\bar{\mu}$ values (but much less in their temperature dependence) we can say that fitting at 300 K is particularly sensitive

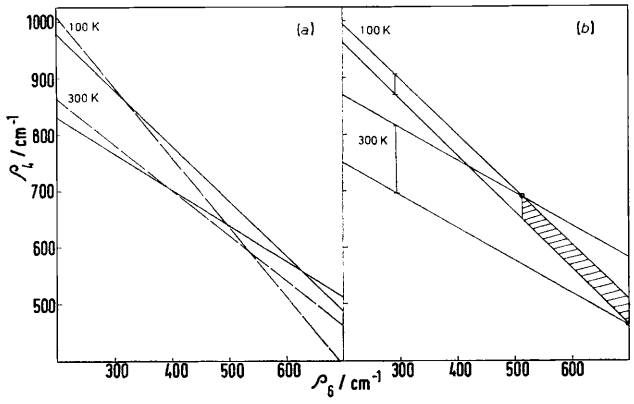

FIGURE 5 (*a*) Relation between ρ_4 and ρ_6 values required to fit mean moments of $Pr(antip)_6I_3$ at 300 and 100 K. Intersections show simultaneous fits at both temperatures. Dotted curves show corresponding behaviour for calculations neglecting intermediate coupling. $\rho_2 = 1500$ cm^{-1}, $\theta = 53°$. (*b*) As for (*a*) with intermediate coupling, but allowing $\pm 1\%$ error in experimental $\bar{\mu}$ values. Points of intersection for $+1\%$ and -1% errors, respectively are indicated by circles. $\rho_2 = 1500$ cm^{-1}, $\theta = 53°$

and moves the 300 K line in Figure 5 in a parallel fashion to and from the origin; *i.e.* sensitivity to ρ_4 and ρ_6 are approximately equal. Accordingly the crossing point is especially sensitive to experimental error. This is shown in Figure 5(*b*) from which we observe a correlation between the fitting value of ρ_4 and ρ_6 as follows:

if	$\rho_4 = 690$	640	580	530	480
then	$\rho_6 = 510$	550	600	650	700

Accordingly, we shall take $\rho_4 = 600 \pm 100$, $\rho_6 = 600 \pm 100$ cm^{-1}.

For the ρ_4 and ρ_6 values we then plot calculated anisotropies $\Delta\mu$ as functions of θ for several ρ_2 values. Two examples are shown in Figure 6 for $\rho_2 = 500$ and 1500 cm^{-1}. Before consideration of the detailed fits to experiment, we draw attention to the unusual temperature dependence *calculated* in this system. Thus $\Delta\mu$(300 K) and $\Delta\mu$(200 K) are nearly identical and larger than $\Delta\mu$(100 K). The usual behaviour for $\Delta\mu$ values in the lanthanide series has been an approximately equal difference in the *reversed* sense, *i.e.* $\Delta\mu(100) > \Delta\mu(200) > \Delta\mu(300)$. The experimental behaviour noted above is thus well reproduced by the same point-charge model we have used throughout this series and we need not invoke any special features like exchange, disorder, *etc.*

The experimental anisotropies for $Pr(antip)_6I_3$ are shown in Figure 6 (the values at 300 and 200 K are approximately equal). From the curves calculated with $\rho_2 = 1500$ cm^{-1} we note that $\theta^f(100) \neq \theta^f(300)$, rather as for the ytterbium compounds [5] except that this small temperature variation is here the other way round, *i.e.* $\theta^f(300\text{ K}) < \theta^f(100\text{ K})$ and so follows the reversed sense of the calculated $\Delta\mu$ curves. This tends to argue against the change in θ^f with temperature being simply related to the onset of phase change as suggested in earlier parts of this series. Presumably, we would have expected the same sense of change of θ^f with temperature regardless of the theoretical 'accident' of reversed temperature dependence of $\Delta\mu$ in Figure 6. The problem is clearly not too important, especially if ρ_2 is very large (2000—3000 cm^{-1}) when $\delta\theta$, the change in fitting θ values with temperature, is always very small. We do not consider as justifiable, the idea of fixing ρ_2 values in this series (which we have not previously been able to do) by finding those values which remove this temperature dependence of θ^f. The answer probably lies in deficiences in the point-charge model in detail, in that any second-co-ordination sphere effects are ignored explicitly: the effect is very small in any case.

It is immediately apparent from curves like those in Figure 6 that fits to experimental anisotropies are only possible for $\rho_2 >$ *ca.* 1000 cm^{-1} but not for $\rho_2 = 500$ cm^{-1}, say. However, since ρ_4 and ρ_6 values were estimated from graphs (Figure 4 and 5) constructed for $\theta = 53°$ as above, and further as any fit for $\rho_2 = 500$ cm^{-1} elsewhere in this series has always occurred when $\theta \lesssim 49°$, the non-acceptibility of $\rho_2 = 500$ cm^{-1} above may be spurious. Accordingly, we constructed Figures

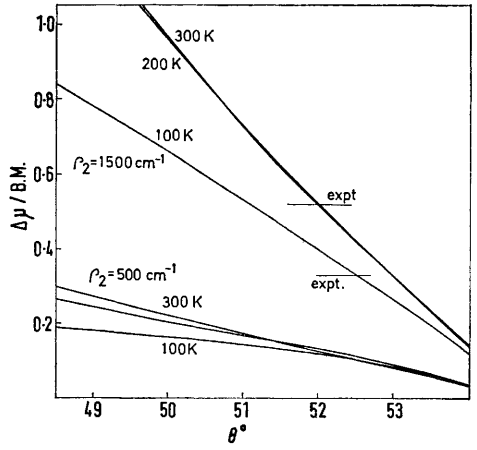

FIGURE 6 Magnetic anisotropies as functions of θ and ρ_2. Experimental values for $Pr(antip)_6I_3$ are indicated by horizontal lines for $T = 300$ and 100 K

like 4 and 5 for $\rho_2 = 500$ cm^{-1}, $\theta = 49°$: even under these conditions no fit is possible, this time because of the impossibility of fitting $\bar{\mu}(300)$ and $\bar{\mu}(300)$ simultaneously for ρ_4 and ρ_6 in the range 0—1500 cm^{-1}. Although for previous members of the series we have not favoured such low ρ_2 values, this appears to be the first case in which we have proved the impossibility of $\rho_2 = 500$ cm^{-1}.

Also as part of the iterative procedures we have investigated the dependence of $\bar{\mu}$ on ρ_2. In previous papers we found essentially no dependence of $\bar{\mu}$ on ρ_2

but these results were for θ values close to 53°. We find for the f^2 case that for θ *ca.* 53° there is virtually nil sensitivity of $\bar{\mu}$ to ρ_2, but for θ *ca.* 50° and at the lower temperatures, $\bar{\mu}$(100 K) changes from 2·44 to 2·71 B.M. as ρ_2 varies from 500 to 2000 cm^{-1}. This is an apparently serious complication: conversely it could be a convenience in that it might offer the possibility of fixing ρ_2 for the first time. However, the anisotropy values remove the difficulty in that θ values must be paired up with ρ_2 values. Comparing μ(100 K) values under circumstances which may fit anisotropies we have the following examples:

$$\left.\begin{array}{l}\rho_2 = 2000\ \text{cm}^{-1} \\ \theta = 53{\cdot}13^\circ\end{array}\right\} \bar{\mu}(100\ \text{K}) = 2{\cdot}38\ \text{B.M.} \left.\begin{array}{l}\\ \\ \\ \end{array}\right\} \bar{\mu}(100\ \text{K}),\ \text{expt} = 2{\cdot}39\ \text{B.M.}$$

$$\left.\begin{array}{l}\rho_2 = 1000 \\ \theta = 51{\cdot}12^\circ\end{array}\right\} \bar{\mu}(100\ \text{K}) = 2{\cdot}43\ \text{B.M.}$$

We should also consider how ρ_4 and ρ_6 estimates may vary with θ. From plots like those in Figures 4 and 5, however, we find that for θ in the range $50{\cdot}5 < \theta < 53{\cdot}5^\circ$, ρ_4 and ρ_6 estimated by the processes discussed above give the same values within the quoted errors. The procedures discussed above therefore appear to cover the peculiarities of the system adequately and were adopted largely on the grounds of minimizing computing time.

Accordingly, we construct Table 5 giving values of θ and $A_2^\circ\langle r^2\rangle$ (related to the coefficient of Y_2° in the potential) corresponding to perfect fits to experimental

TABLE 5

Pr(antip)$_6$I$_3$: values of ρ_2, θ, and $A_2^\circ\langle r^2\rangle$ to fit anisotropies $\rho_4 = 600$ cm^{-1}, $\rho_6 = 600$ cm^{-1}, $A_2^\circ\langle r^2\rangle = \frac{3}{2} \cdot \rho_2(3\cos^2\theta - 1)$

Experimental values: $\bar{\mu}(300\ \text{K}) = 3{\cdot}33$, $\bar{\mu}(200\ \text{K}) = 3{\cdot}08$, $\bar{\mu}(100\ \text{K}) = 2{\cdot}39$ B.M.

T/K	θ°	$A_2^\circ\langle r^2\rangle$/cm^{-1}	$\bar{\mu}$(calc)/B.M.
$\rho_2 = 1000$ cm^{-1}			
300	50·45	324	3·35
200	50·32	335	3·11
100	51·12	274	2·43
$\rho_2 = 1500$ cm^{-1}			
300	52·00	309	3·33
200	51·95	311	3·08
100	52·55	246	2·40
$\rho_2 = 2000$ cm^{-1}			
300	52·75	297	3·32
200	52·75	297	3·06
100	53·13	239	2·38

anisotropies at 300, 200, and 100 K for various ρ_2 values. Also given are the associated, calculated $\bar{\mu}$ values which all agree very well with experiment. As ρ_2 is taken from 1000 to 2000 cm^{-1}, $A_2^\circ\langle r^2\rangle$ values are moderately constant, decreasing by only 10—20%.

Thus summarizing, the praseodymium compound in this series of six-co-ordinate lanthanide complexes appears exceptional in a number of ways. It is encouraging to see that the simple D_{3d}, point-charge crystal-field model we have used throughout the series successfully reproduces the 'unusual' temperature variation observed for the crystal anisotropy. Those interested may trace this behaviour back to the energy levels shown in Figure 2 and the consequent principal moments in Figure 3(*b*). In all previous cases in this series the curvature of the principal moments with respect to θ at 100 K were considerably greater than at 300 K. In the region $49 < \theta < \theta_{oct}$ the reverse is true for f^2 ions. Associated with this we have found a greater dependence of $\bar{\mu}$(100 K) on θ which has necessitated a more lengthy fitting process than previously. However, the most important anomaly of Pr(antip)$_6$I$_3$ is the approximate equality of the values estimated for ρ_4 and ρ_6 at *ca.* 600 cm^{-1}: this follows despite the estimated errors which might give the ratio ρ_4/ρ_6 anywhere in the range 1·4—0·7. We hope to comment upon this on completion of the series. Finally, we have found $A_2^\circ\langle r^2\rangle$ to lie in the range 290 ± 50 cm^{-1}.

APPENDIX

The eigenvectors for the six lowest states corresponding to the eigenvalues of Runciman and Wybourne [3] given in Table 1 are as follows:

Label	Vector
$^3H_4$	$0{\cdot}9879\ \|^3H_4\rangle - 0{\cdot}0283\ \|^3F_4\rangle + 0{\cdot}1523\ \|^1G_4\rangle$
$^3H_5$	$1{\cdot}0000\ \|^3H_5\rangle$
$^3H_6$	$0{\cdot}9985\ \|^3H_6\rangle - 0{\cdot}0540\ \|^1I_6\rangle$
$^3F_2$	$0{\cdot}9894\ \|^3F_2\rangle + 0{\cdot}1443\ \|^1D_2\rangle - 0{\cdot}0132\ \|^3P_2\rangle$
$^3F_3$	$1{\cdot}0000\ \|^3F_3\rangle$
$^3F_4$	$0{\cdot}1009\ \|^3H_4\rangle + 0{\cdot}8634\ \|^3F_4\rangle - 0{\cdot}4943\ \|^1G_4\rangle$

Based on these, we have calculated correction factors for the crystal-field reduced matrix elements when used with pure Russell–Saunders state wavefunctions, as in ref. 7. They are as follows:

$U2$ $U4$ $U6$	$^3H_4$	$^3H_5$	$^3H_6$	$^3F_2$	$^3F_3$	$^3F_4$
$^3H_4$	0·9782 1·0353 0·8697					
$^3H_5$	1·0107 0·9508 1·0228	1·0000 1·0000 1·0000				
$^3H_6$	0·2833 1·2544 0·9492	0·9985 0·9985 0·9985	1·0028 0·9926 0·9958			
$^3F_2$	1·0088 0·9845 0·9209	0 1·0000 0·9951	0 0·8961 1·0017	1·0593 0·7183 0		
$^3F_3$	0·9710 0·9765 0·9953	1·0000 1·0000 0	0 0·9985 0·9985	0·9437 1·0237 0	1·0000 1·0000 1·0000	
$^3F_4$	2·4170 0·9398 1·0763	0·7383 0·9404 0·7816	0·8840 0·8877 0·8760	1·1228 0·4164 1·0768	1·0327 1·1135 0·4786	0·5320 1·6270 −0·6728

We thank the S.R.C. for a post-doctoral research grant (to D. J. M.).

[1/1562 *Received, August 26th,* 1971]

[7] M. Gerloch and D. J. Mackey, *J. Chem. Soc.* (*A*), 1971, 3372.